Supplementary Information

A mitochondrial pathway for biosynthesis of lipid mediators.

Yulia Y. Tyurina[1,2]*, Samuel M. Poloyac[3], Vladimir A. Tyurin[1,2], Alexander A. Kapralov[1,2], Jianfei Jiang[1,2] ,Tamil Selvan Anthonymuthu[1,4], Valentina I. Kapralova[1,2], Anna S. Vikulina[1,2,7], Mi-Yeon Jung[1,2], Michael W. Epperly[5], Dariush Mohammadyani[6], Judith Klein-Seetharaman[8], Travis C. Jackson[4], Patrick M. Kochanek[4], Bruce R. Pitt[2,6], Joel S. Greenberger[5], Yury A. Vladimirov[7], Hülya Bayır[1,4]*, Valerian E. Kagan[1,2]*

[1]Center for Free Radical and Antioxidant Health, [2]Department of Environmental Health, Graduate School of Public Health,

[3]Department of Pharmaceutical Sciences, School of Pharmacy,

[4]Departments of Critical Care Medicine, Safar Center for Resuscitation Research,

[5]Radiation Oncology, School of Medicine, [6]Department of Bioengineering, Swanson School of Engineering, University of Pittsburgh, Pittsburgh PA 15213, USA,

[7]Department of Biophysics, MV Lomonosov Moscow State University, Moscow, Russia,

[8]Division of Metabolic and Vascular Health, University of Warwick, Coventry CV4 7AL, UK.

Supplementary Results

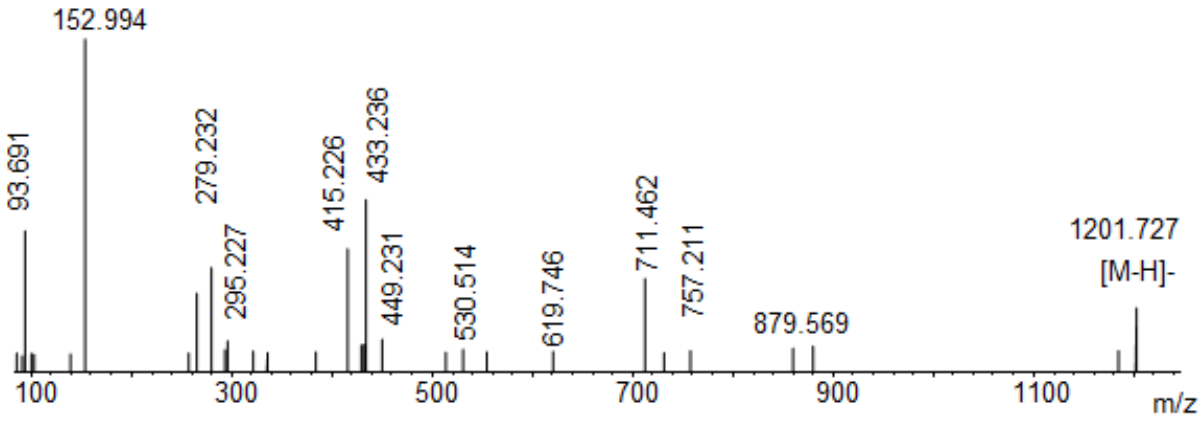

Figure S1a. MS/MS spectrum of mCL molecular species with m/z 1201.727 ($C_{63}H_{111}O_{17}P_2$) obtained from the small intestine of mice expose to WBI (10 Gy, 10hrs after WBI). mCL was separated by 2D-HPTLC and analyzed by reverse phase LC/MS (C8 column) using orbitrap QExactive mass spectrometer (ThermoFisher Scientific, San Jose, CA). MS/MS fragmentation reveals the presence of mCL containing mono-oxygenated LA (m/z 295.227).

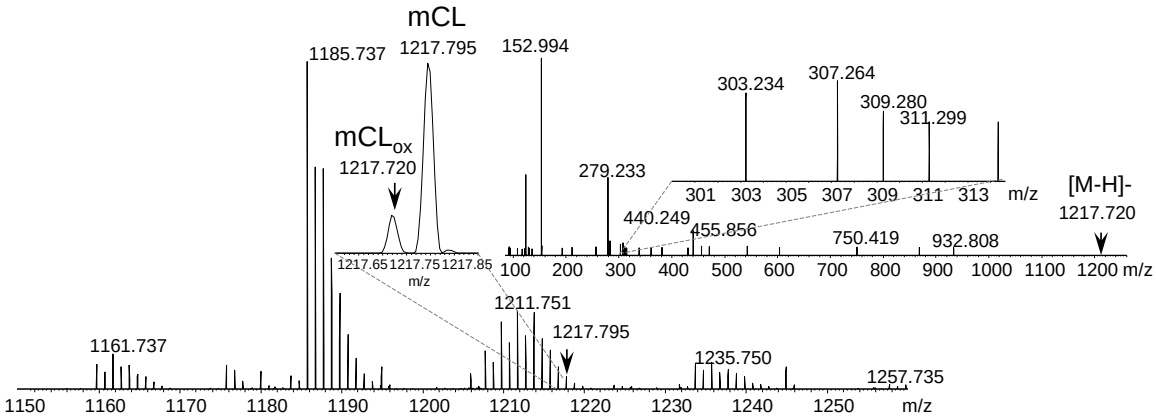

Figure S1b. Full MS spectrum of mCL obtained from the small intestine of mice exposed to WBI (10 Gy, 10 hrs after WBI). mCL was analyzed by normal phase LC/MS using orbitrap QExactive mass spectrometer (ThermoFisher Scientific, San Jose, CA. Inserts: Left: Part of the MS spectrum in m/z range from 1217.65 to 1217.85. mCL (m/z 1217.795) and mCL_{ox} (m/z 1217.720) were completely resolved. Right: MS/MS spectrum of mCL di-oxygenated molecular species with m/z 1217.720 ($C_{63}H_{111}O_{18}P_2$). MS/MS fragmentation reveals the presence of mCL containing di-oxygenated LA (m/z 311.299).

Table S1. Mono-lysoCLs detected *in vivo* in rat brain and mouse small intestine.

m/z	Formula	mCL molecular species	CCI	WBI
1135.720	$C_{59}H_{109}O_{16}P_2$	(C16:0)(C16:1)(C18:2)	+	+
1137.735	$C_{59}H_{111}O_{16}P_2$	(C16:0)(C16:1)(C18:1)	+	+
1157.704	$C_{61}H_{107}O_{16}P_2$	(C16:1)(C16:1)(C20:4)	+	
1159.722	$C_{61}H_{109}O_{16}P_2$	(C18:2)(C16:1)(C18:2)	+	+
		(C16:1)(C16:0)(C20:4)	+	+
1161.735	$C_{61}H_{111}O_{16}P_2$	(C18:1)(C16:1)(C18:2)	+	+
		(C16:0)(C16:0)(C20:4)	+	+
1163.751	$C_{61}H_{113}O_{16}P_2$	(C18:1)(C16:0)(C18:2)	+	+
		(C18:0)(C16:1)(C18:2)	+	
1165.766	$C_{61}H_{115}O_{16}P_2$	(C16:0)(C18:0)(C18:2)		+
		(C16:0)(C18:1)(C18:1)	+	+
		(C16:1)(C18:0)(C18:1)	+	
1185.735	$C_{63}H_{111}O_{16}P_2$	(C18:2)(C18:2)(C18:2)	+	+
		(C16:0)(C18:2)(C20:4)	+	+
		(C16:1)(C18:1)(C20:4)	+	
1187.75	$C_{63}H_{113}O_{16}P_2$	(C18:2)(C18:2)(C18:1)	+	+
		(C16:0)(C18:1)(C20:4)	+	+
		(C16:1)(C18:0)(C20:4)	+	
1189.765	$C_{63}H_{115}O_{16}P_2$	(C18:1)(C18:1)(C18:2)	+	+
		(C16:0)(C18:0)(C20:4)	+	
1191.782	$C_{63}H_{117}O_{16}P_2$	(C18:1)(C18:1)(C18:1)	+	+
		(C18:1)(C18:0)(C18:2)		+
		(C18:0)(C18:1)(C18:2)	+	
1193.725	$C_{61}H_{111}O_{18}P_2$	(C16:0)(C18:2)(C18:2+2O)	+	
1199.715	$C_{63}H_{109}O_{17}P_2$	(C18:2)(C18:2)(C18:2+O*)		+
1201.73	$C_{63}H_{111}O_{17}P_2$	(C18:2)(C18:2)(C18:2+O$^{\#}$)		+
1203.746	$C_{63}H_{113}O_{17}P_2$	(C18:1)(C18:2)(C18:2+O$^{\#}$)		+
1207.72	$C_{65}H_{109}O_{16}P_2$	(C18:3)(C18:2)(C20:4)		+
1209.736	$C_{65}H_{111}O_{16}P_2$	(C18:2)(C18:2)(C20:4)	+	
		(C16:1)(C18:1)(C22:6)	+	+
1211.751	$C_{65}H_{113}O_{16}P_2$	(C16:0)(C20:3)(C20:4)	+	+
		(C18:1)(C18:2)(C20:4)	+	+
		(C16:0)(C18:1)(C22:6)	+	

1213.767	$C_{65}H_{115}O_{16}P_2$	(C18:1)(C18:1)(C20:4)	+	+
		(C18:0)(C18:2)(C20:4)	+	+
1215.781	$C_{65}H_{117}O_{16}P_2$	(C18:1)(C18:2)(C20:2)		+
		(C18:1)(C18:0)(C20:4)	+	
1215. 709	$C_{63}H_{109}O_{18}P_2$	(C16:1)(C20:4)(C18:2+2O)	+	
1217.725	$C_{63}H_{111}O_{18}P_2$	(C18:2)(C18:2)(C18:2+2O)	+	+
1217.795	$C_{65}H_{119}O_{16}P_2$	(C18:0)(C18:0)(C20:4)	+	
1233.736	$C_{67}H_{111}O_{16}P_2$	(C18:2)(C20:4)(C20:4)	+	+
		(C18:2)(C18:2)(C22:6)		+
		(C16:0)(C20:4)(C22:6)	+	
1235.75	$C_{67}H_{113}O_{16}P_2$	(C18:2)(C18:2)(C22:5)		+
		(C18:1)(C18:2)(C22:6)	+	+
		(C16:0)(C20:3)(C22:6)	+	
		(C18:1)(C20:4)(C20:4)	+	
1237.766	$C_{67}H_{115}O_{16}P_2$	(C18:1)(C18:1)(C22:6)	+	+
		(C18:0)(C18:2)(C22:6)	+	
		(C16:0)(C20:4)(C22:4)	+	
1239.78	$C_{67}H_{117}O_{16}P_2$	(C18:2)(C20:3)(C20:2)		+
		(C18:1)(C18:0)(C22:6)	+	+
1257.735	$C_{69}H_{111}O_{16}P_2$	(C20:4)(C20:4)(C20:4)	+	+
		(C18:2)(C20:4)(C22:6)	+	+

* oxo functional group

hydroxy or epoxy functional group

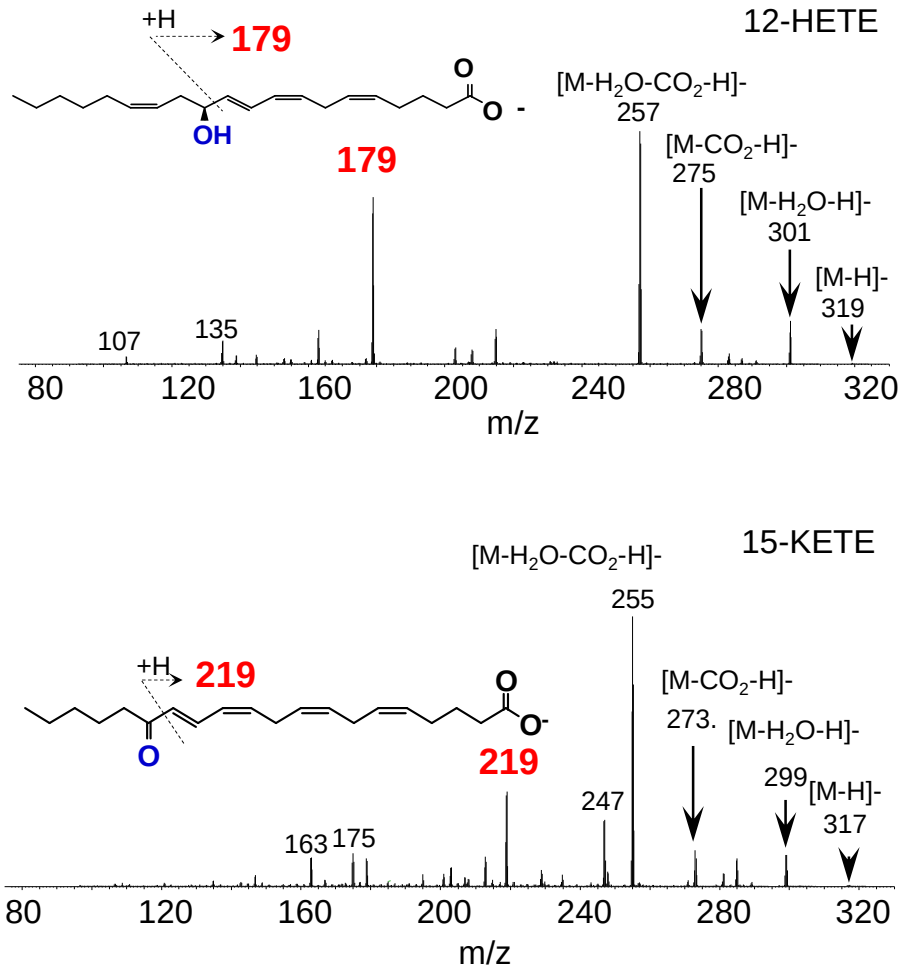

Figure S2. MS/MS spectra of AA_{ox} molecular ions with m/z 317 (low panel) and 319 (upper panel) formed in the small intestine 10 hrs after WBI (10 Gy). AA_{ox} were analyzed and quantitatively assessed by reverse phase (C18 column) LC/MS using LXQ ion trap mass spectrometer (ThermoFisher Scientific, San Jose, CA). Oxygenated species of AA were identified as mono-hydroxy-AA (12-HETE) and oxo-AA (15-KETE).

Table 2. Fatty acid oxygenated products formed in CL exposed to cyt c/H_2O_2.

m/z	Name	Abbreviation	CCl	WBI	Function
293	9-oxo-octadecadienoic acid	9-KODE	+	+	TRPV1 endogenous ligand[1]
293	13-oxo-octadecadienoic acid	13-KODE	+	+	Activation of PPARγ [2] TRPV1 endogenous ligand [1]
295	9-hydroxy-octadecadienoic acid	9-HODE	+	+	Pro-inflammatory[3], TRPV1 endogenous ligand[4], G2A receptor ligand[5]
295	13-hydroxy-octadecadienoic acid	13-HODE	+	+	Anti-inlammatory[3], Activation of PPARγ , ↓IL-8; ABCA1 expression; TRPV1 endogenous ligand[4]
295	9,10-epoxy-octadecanoic acid	9,10-EpOME	+		
295	12,13-epoxy-octadecanoic acid	12,13-EpOME	+		
309	9-oxo,14-hydroxy-octadecadienoic acid	9,14-KHODE	+		
309	8-hydroxy, 13-oxo-octadecadienoic acid	8,13-HKODE	+		
309	9,10-epoxy, 13-oxo-octadecanoic acid	9,10,13-EpKOME			
309	9-oxo, 12,13-epoxy-octadecanoic acid	9,12,13-KEpOME			Aldosteronogenesis[6]
309	9,10-epoxy, 13-hydroxy-octadecanoic acid	9,10,13-EpHOME			
309	9-hydroxy, 12,13-epoxy-octadecanoic acid	9,12,13-HEpOME			
311	9-hydroperoxy-octadecadienoic acid	9-HpODE	+	+	
311	13-hydroperoxy-octadecadienoic acid	13-HpODE		+	
311	8,13-dihydroxy-octadecadienoic acid	8,13-DiHODE	+		
311	9,14-dihydroxy-octadecadienoic acid	9,14-DiHODE			
325	8-oxo,13-hydroperoxy-octadecadienoic acid	8,13-KHpODE	+		
325	8-hydroperoxy, 13-oxo-octadecadienoic acid	8,13-HpKODE	+		
325	9-oxo,14-hydroperoxy-octadecadienoic acid	9,14-KHpODE	+		
325	9-hydroperoxy, 14-oxo-octadecadienoic acid	9,14-HpKODE	+		
327	9-hydroperoxy, 12,13-epoxy-octadecanoic acid	9,12,13-HpEpOME	+	+	PPARγ activation [7, 8]; CD36 expression ; Atherosclerosis[9], Apoptosis[10], Vasodilation[11], Vasoconstriction[11], Platelet aggregation[12]
317	15-oxo-eicosatetraenoic acid	15-KETE		+	
319	15-hydroxy-eicosatetraenoic acid	15-HETE		+	
319	12-hydroxy-eicosatetraenoic acid	12-HETE	+	+	Atherosclerosis[9], Mitogenesis[10], Angiogenesis[10], Vasoconstriction[13], Vasodilation, Platelet aggregation[12]
319	14,15-epoxy-eicosatrienoic acid	14,15-EpETrE			Vasodilation[14], Angiogenesis[14], Anti-inflammatory[15], Anti-platelet[15]
319	11,12-epoxy-eicosatrienoic acid	11,12-EpETrE			Vasodilation[14], Angiogenesis[14], Anti-inflammatory[15], Anti-platelet[15]
319	8,9-epoxy-eicosatrienoic acid	8,9-EpETrE			Vasodilation[14], Angiogenesis[14], Anti-inflammatory[15], Anti-platelet[15].
337	8,9-dihydroxy-eicosatrienoic acid	8,9-DiHETrE			
337	5,6-dihydroxy-eicosatrienoic acid	5,6-DiHETrE			
337	11,12-dihydroxy-eicosatrienoic acid	11,12-DiHETrE			
337	14,15-dihydroxy-eicosatrienoic acid	14,15-DiHETrE			
293	Truncated 4,10,16-trihydroxy-docosahexanaenoic acid				
265	Truncated 14,15-DiHETrE				

Table S3. Effect of inhibitors of cyclooxygenase, lipoxygenase, cytochrome P-450 and mitochondrial Ca^{2+}-independent phospholipase $A_2\gamma$ on peroxidase activity of cyt *c* /TOCL complexes.

Name of inhibitor	Activity, % of control (cyt *c*/TOCL)
None	100+6.8
R-BEL	98.8+2.1
Piroxicam	91.9+4.6
MS-PPOH	97.9+2.4
Licophelone	88.4+3.3

Cyt *c*/TOCL ratio is 20:1, inhibitors/cyt *c* ratio is 3:1. Data are Mean ± SD; N=6

Table S4. Effect of COX/LOX/P-450 inhibitors on irradiation induced accumulation of oxygenated FA in mouse small intestine.

	WBI	WBI+COX/LOX/P450 Inhibitors
12-HETE	100.0 ± 6.1	43.3 ± 6.8
15-HETE	100.0 ± 13.0	40.0 ± 7.5
15-KETE	100.0 ± 16.0	34.8 ± 8.6
PGE2	100.0 ± 18.0	27.3 ± 9.7
PGD2	100.0 ± 16.0	48.9 ± 19.0
HODE	100.0 ± 13.0	45.2 ± 8.0
Di-HODE	100.0 ± 17.0	120.0 ± 39.0
KODE	100.0 ± 21.0	22.0 ± 5.9

Mice were treated with a mixture of inhibitors (piroxicam, 30 mg/kg of body weight; licophelone, 10 mg/kg of body weight and MS-PPOH, 25 mg/kg of body weight) by oral gavage 2 hrs prior to irradiation. Control mice and mice pretreated with drugs were exposed to WBI (10Gy) and sacrificed 24 hrs thereafter. Data are presented as % of particular FA_{ox} accumulated in irradiated non-treated mice. Data are Mean ± SD; N=6-8.

R-BEL, 6E-(bromoethylene)tetrahydro-3R-(1-naphthalenyl)-2H-pyran-2-one, (R)-bromoenol lactone) - an inhibitor of Ca^{2+}-independent $iPLA_2g$ *in vivo*; Piroxicam, (4-hydroxy-2-methyl-N-2-pyridinyl-2H-1,2-benzothiazine-3-carboxam, ide-1,1-dioxide) - inhibitor of COX-1 and COX-2 ;MS-PPOH, (N-(methylsulfonyl)-2-(2-propynyloxy)-benzenehexanamide)-inhibitor of cytochrome P450; Licofelone (6-(4-chlorophenyl)-2,3-dihydro-2,2-dimethyl-7-phenyl-1H-pyrrolizine-5-acetic acid)- dual COX/5-LOX inhibitor

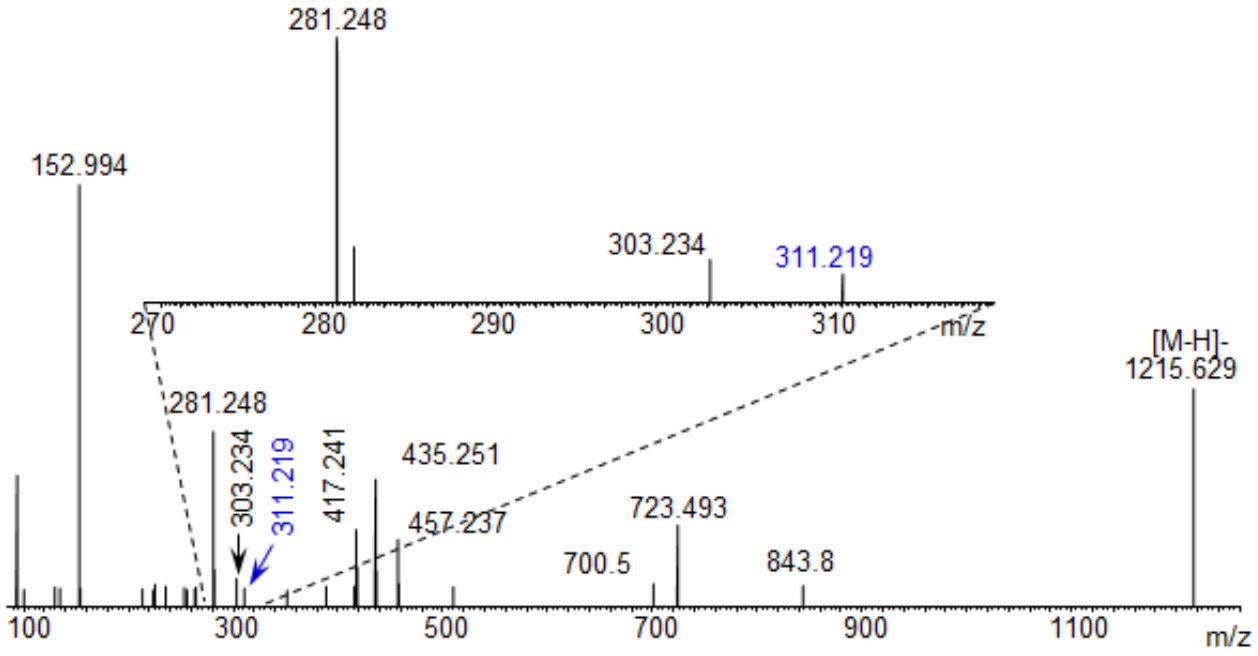

Figure S3. MS/MS spectrum of mCL molecular species with m/z 1215.629 ($C_{63}H_{109}O_{18}P_2$) obtained from rat brain after CCI. mCL was separated by 2D-HPTLC and analyzed by reverse phase (C8 column) LC/MS using orbitrap QExactive mass spectrometer (ThermoFisher Scientific, San Jose, CA). MS/MS fragmentation reveals the presence of CL_{ox} containing di-oxygenated LA (m/z 311.219).

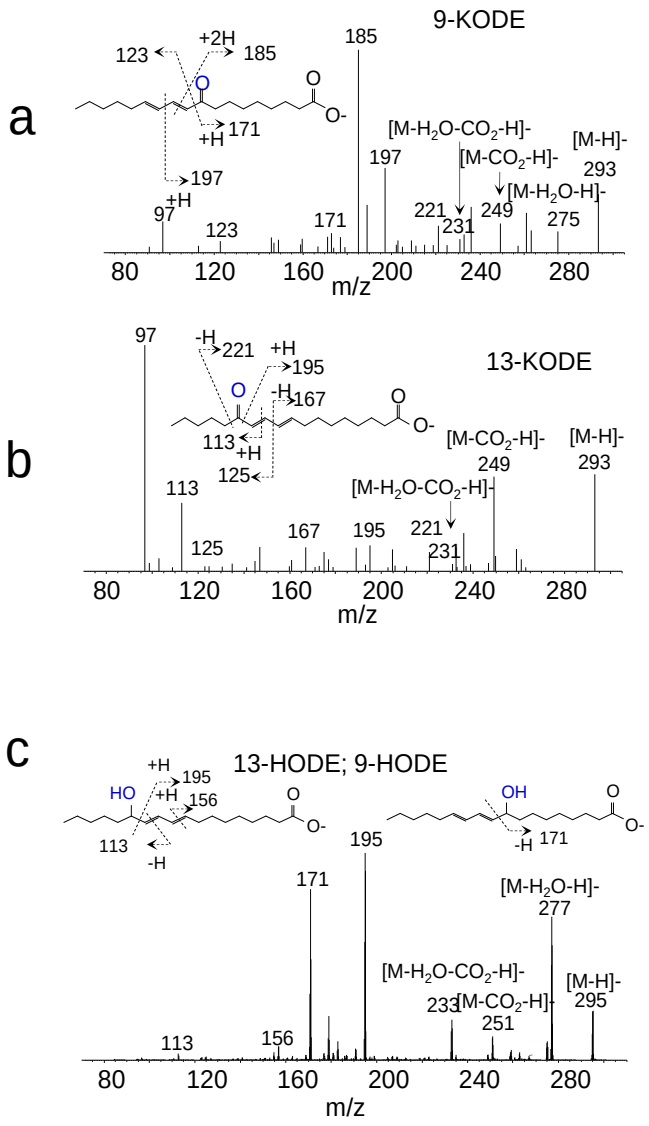

Figure S4. MS/MS spectra of AA_{ox} molecular ions with m/z 293 (a,b), and 295 (c) formed in brain after CCI. $PUFA_{ox}$ were analyzed and quantitatively assessed by reverse phase (C18 column) LC/MS by using LXQ ion trap mass spectrometer (ThermoFisher Scientific, San Jose, CA). Oxygenated species of LA with m/z 293 were identified as keto-LA (9-KODE and 13-KODE). Species with m/z 295 were characterized as mono-hydroxy-LA (9-HODE and 13-HODE).

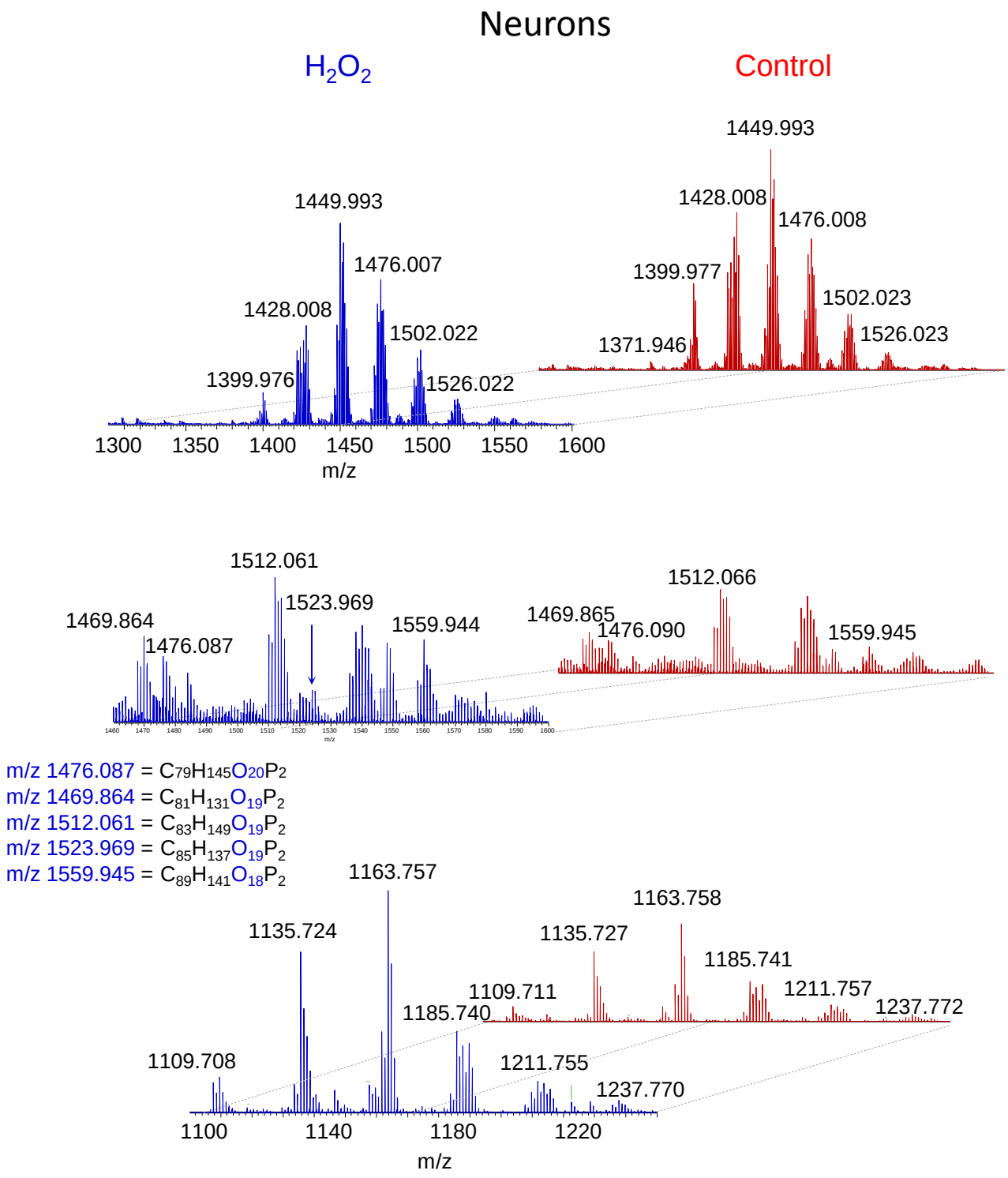

Figure S5. Mass spectra of CL (upper panels), CL_{ox} (middle panels) and mCL (lower panel) obtained from primary cortical rat neurons before (red) and after (blue) treatment with H_2O_2.

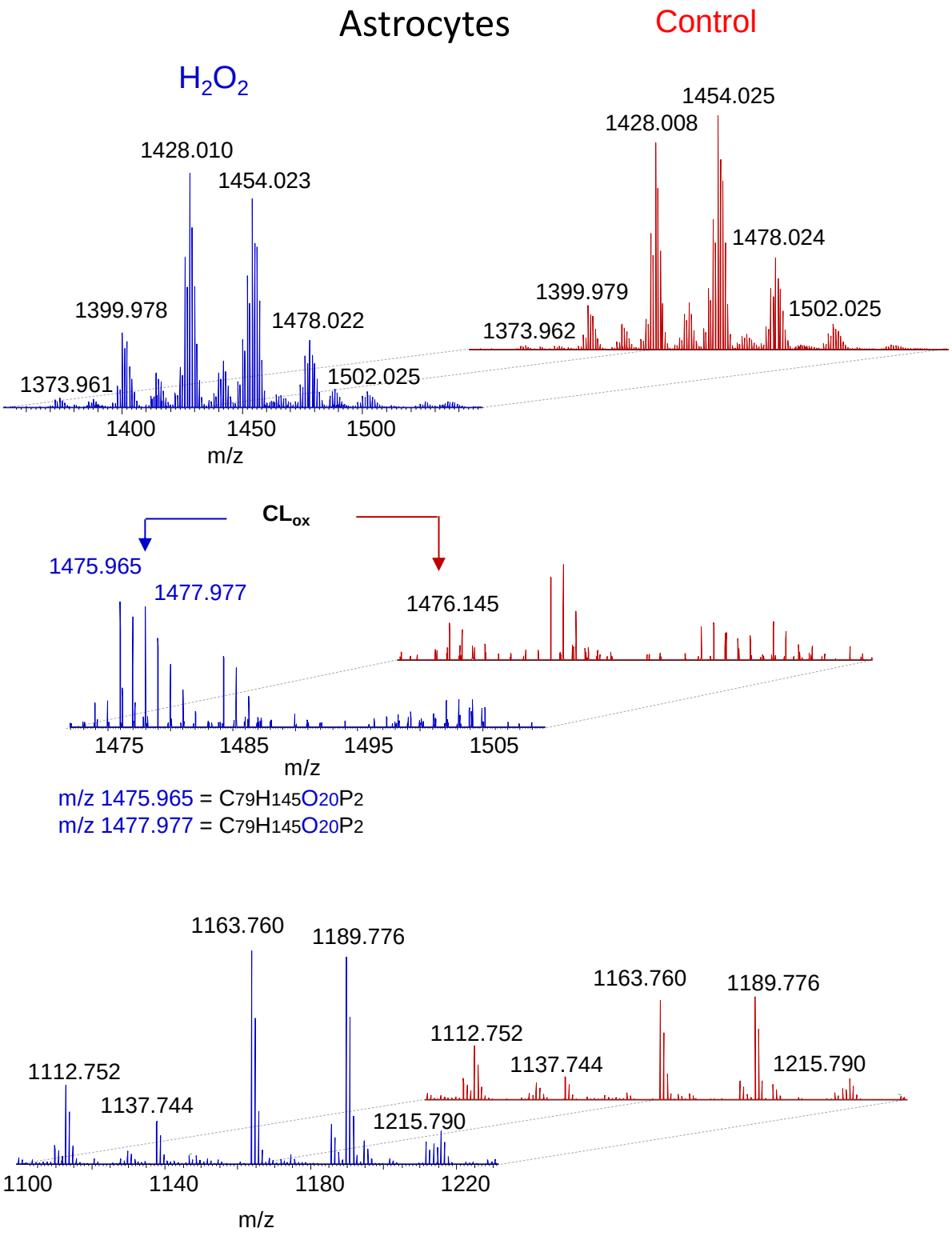

Figure S6. Mass spectra of CL (upper panels), CL_{ox} (middle panels) and mCL (lower panels) obtained from primary rat cortical astrocytes before (red) and after (blue) treatment with H_2O_2.

Table S5. Cardiolipin molecular species from rat neurons and astrocytes.

m/z	Formula	Acyl chain Total Carbon: No. of Double bond	Astrocyte	Neurons
1401.981	$C_{77}H_{144}O_{17}P_2$	68:3	+	+/↓
1399.965	$C_{77}H_{142}O_{17}P_2$	68:4	+	+/↓
1397.949	$C_{77}H_{140}O_{17}P_2$	68:5	+	+/↓
1395.934	$C_{77}H_{138}O_{17}P_2$	68:6	ND	+/↓
1393.918	$C_{77}H_{136}O_{17}P_2$	68:7	ND	+/↓
1432.028	$C_{79}H_{150}O_{17}P_2$	70:2	+	
1430.012	$C_{79}H_{148}O_{17}P_2$	70:3	+	+/↓
1427.996	$C_{79}H_{146}O_{17}P_2$	70:4	+	+/↓
1425.981	$C_{79}H_{144}O_{17}P_2$	70:5	+	+/↓
1423.965	$C_{79}H_{142}O_{17}P_2$	70:6	+	+/↓
1421.949	$C_{79}H_{140}O_{17}P_2$	70:7	+	+/↓
1419.934	$C_{79}H_{138}O_{17}P_2$	70:8	ND	+/↓
1443.934	$C_{81}H_{138}O_{17}P_2$	72:10	ND	+/↓
1458.043	$C_{81}H_{152}O_{17}P_2$	72:3	+	
1456.028	$C_{81}H_{150}O_{17}P_2$	72:4	+	+/↓
1454.012	$C_{81}H_{148}O_{17}P_2$	72:5	+	+/↓
1451.996	$C_{81}H_{146}O_{17}P_2$	72:6	+	+/↓
1449.981	$C_{81}H_{144}O_{17}P_2$	72:7	+	+/↓
1447.965	$C_{81}H_{142}O_{17}P_2$	72:8	+	+/↓
1445.949	$C_{81}H_{140}O_{17}P_2$	72:9	+	+/↓
1471.965	$C_{83}H_{142}O_{17}P_2$	74:10	+	+/↓
1469.949	$C_{83}H_{140}O_{17}P_2$	74:11	+	+/↓
1482.043	$C_{83}H_{152}O_{17}P_2$	74:5	+/↓	+/↓
1480.028	$C_{83}H_{150}O_{17}P_2$	74:6	+/↓	+/↓
1478.012	$C_{83}H_{148}O_{17}P_2$	74:7	+/↓	+/↓
1475.996	$C_{83}H_{146}O_{17}P_2$	74:8	+/↓	+/↓
1473.981	$C_{83}H_{144}O_{17}P_2$	74:9	+/↓	+/↓
1499.996	$C_{85}H_{146}O_{17}P_2$	76:10	+/↓	+/↓
1497.981	$C_{85}H_{144}O_{17}P_2$	76:11	ND	+/↓
1495.965	$C_{85}H_{142}O_{17}P_2$	76:12	ND	+/↓
1502.012	$C_{85}H_{148}O_{17}P_2$	76:9	+/↓	+/↓
1526.012	$C_{87}H_{148}O_{17}P_2$	78:11	ND	+/↓
1523.996	$C_{87}H_{146}O_{17}P_2$	78:12	ND	+/↓

"+" Indicates the presence of CL molecular species.

↓ Indicates the decrease of CL species upon treatment with H_2O_2.

Changes less than 5% were not considered. ND – not detectable

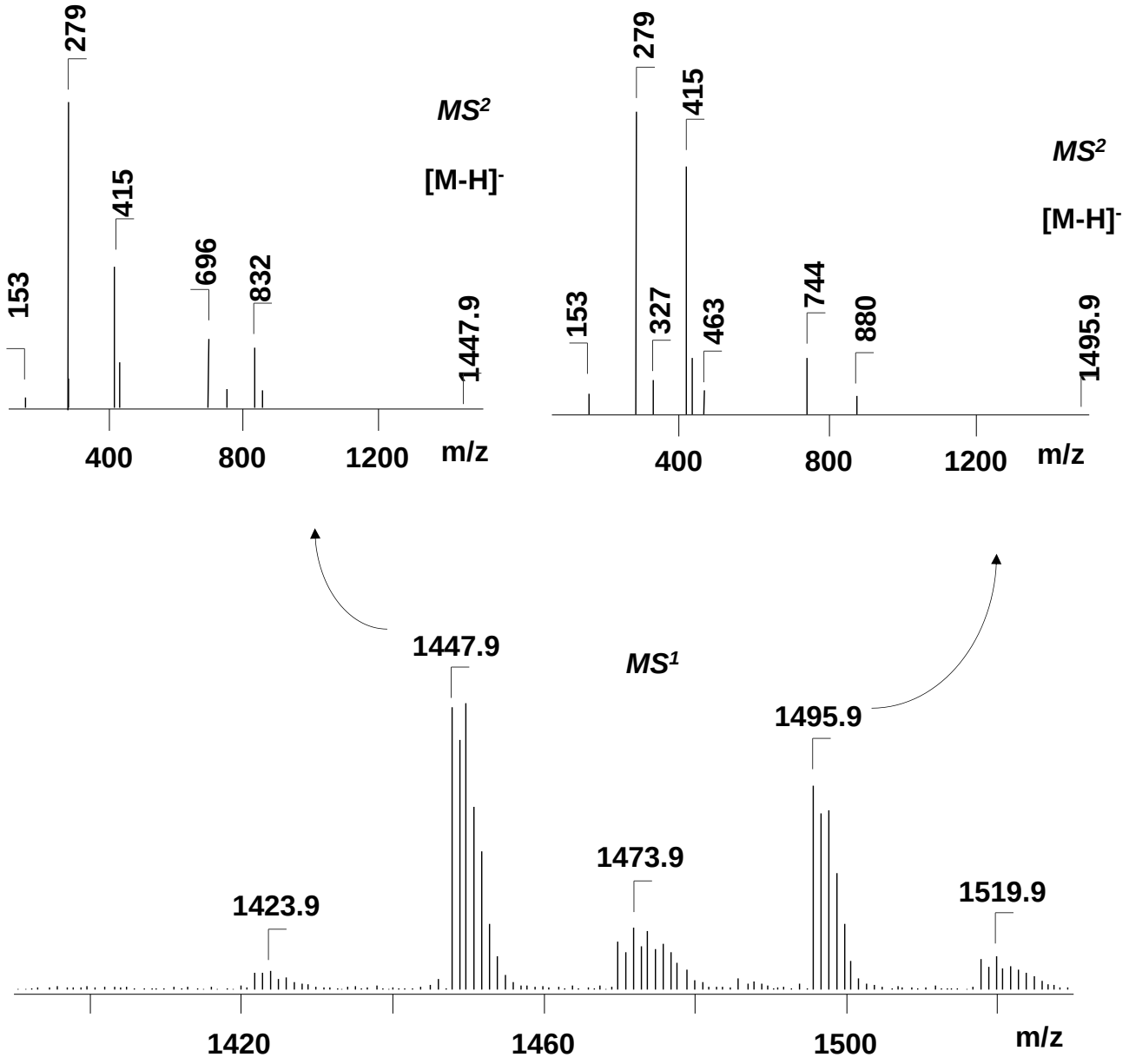

Figure S7. Typical negative ESI-MS spectrum of CL and MS/MS spectra of non-oxidized (*m/z* 1447.9) and oxidized (*m/z* 1495.9) molecular species of CL isolated from heart mitochondria treated with *t*-BuOOH (150μM). ESI-MS analysis demonstrated that CL was represented by at least 5 molecular clusters with *m/z* 1423.9, (1.8%), *m/z* 1447.9, (19.8%), *m/z* 1449.9, (28.8%), *m/z* 1451.9, (4.1%), *m/z* 1475.9 (4%), *m/z* 1495.9 (27.5%) and *m/z* 1497.9 (14%) corresponding to CL molecular species $(C_{18:2})_3/(C_{16:0})_1$, $(C_{18:2})_4$, $(C_{18:2})_3/(C_{18:1})_1$, $(C_{18:2})_2/(C_{18:1})_2$, $(C_{18:2})_2/(C_{18:1})_1/(C_{20:3})_1$, $(C_{18:2})_3/(C_{22:6})_1$, and $(C_{18:2})_2/(C_{18:1})_1/(C_{22:6})_1$, respectively.

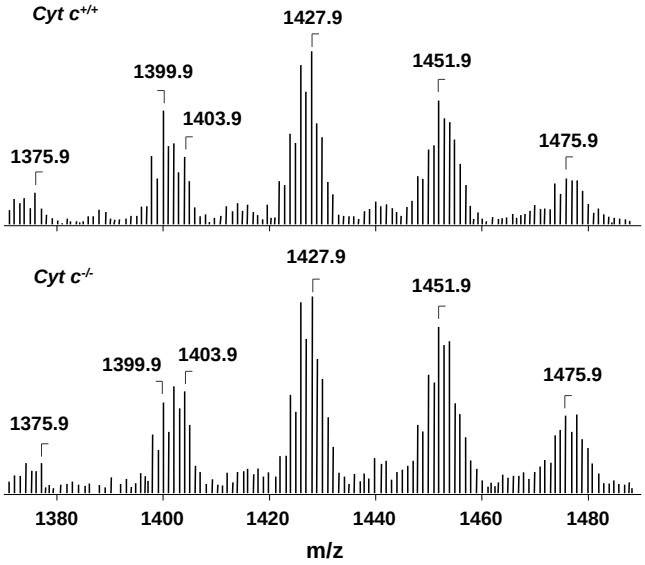

Figure S8a. Typical negative ESI-MS spectra of CL isolated from cyt $c^{+/+}$ and cyt $c^{-/-}$ cells. LC/MS analysis showed that the amount and the diversity of CL molecular species in cyt $c^{+/+}$ and cyt $c^{-/-}$ cells were similar and included the following major molecular species: $(C_{14:0})_1/(C_{16:1})_2/(C_{20:0})_1$, $(C_{16:0})_2/(C_{18:1})_2$, $(C_{18:2})_2/(C_{18:1})_1/(C_{16:0})_1$, $(C_{18:2})_4$, $(C_{18:2})_2/(C_{18:1})_2$, $(C_{18:1})_3/(C_{18:2})_1$, and $(C_{18:2})_2/(C_{18:1})_1/(C_{20:3})_1$.

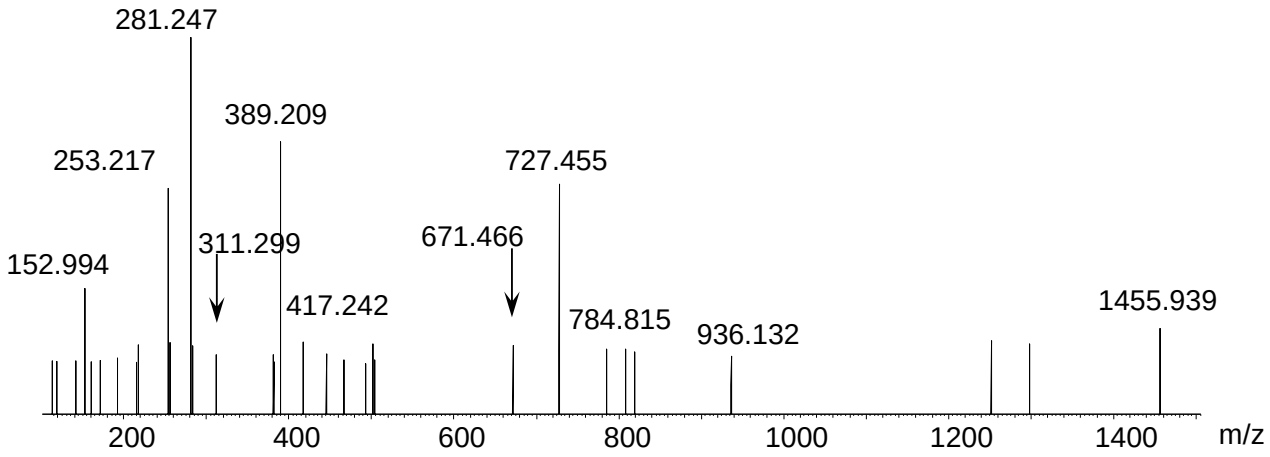

Figure S8b. MS/MS spectrum of CL molecular species with m/z 1455.939 ($C_{79}H_{141}O_{19}P_2$) obtained from cyt $c^{+/+}$ cells expose to AcD (100 ng/ml, 16 hrs). CL was separated by 2D-HPTLC and analyzed by reverse phase LC/MS (C8 column) using orbitrap QExactive mass spectrometer (ThermoFisher Scientific, San Jose, CA). MS/MS analysis of CL_{ox} molecular species with m/z 1455.939 containing di-oxygenated linoleic acid (m/z 311.299).

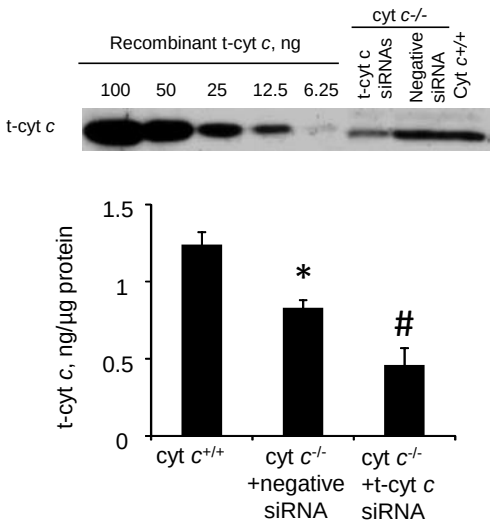

Figure S9a. Quantitative analysis of t-cyt *c* in wild type (cyt $c^{+/+}$) and s-cyt *c* deficient (cyt $c^{-/-}$) cells using western blotting (upper panel). Whole cell lysates were obtained by re-suspending cells in RIPA buffer for 30 min on ice. Supernatants were collected after 5 min centrifugation at 6,000 × g. Recombinant t-cyt *c* was from Creative Biomart (Shirley, NY). Samples were probed with rabbit anti-t-cyt *c* antibody (courtesy of Drs. J.L. Millan and S. Narisawa, Sanford-Burnham Medical Research Institute, LaJolla, CA). Quantification of band intensity was performed using ImageJ pixel analysis (NIH Image software, Ver. 1.47). The cellular content of t-cyt *c* was calculated based on the calibration, and normalized to the amount of protein loaded (means ± SD, n=3) (lower panel). Note that different amounts of protein were loaded: cyt $c^{-/-}$ (30 µg), cyt $c^{-/-}$ with knock-down t-cyt *c* (30µg) and cyt $c^{+/+}$ (20 µg), *p<0.05 vs. cyt $c^{+/+}$, #p<0.05 vs cyt $c^{-/-}$ cells transfected with non-targeting (negative control) siRNA).

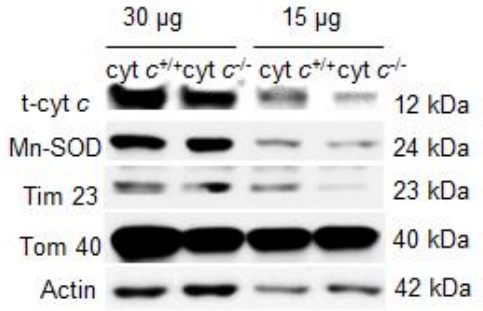

Figure S9b. Assessment of mitochondrial components in wild type (cyt $c^{+/+}$) and somatic cyt *c* deficient (cyt $c^{-/-}$) mouse embryonic cells by western blotting. Mouse anti-Mn-SOD antibody and anti-Tim23 antibody were from BD Pharmingen (San Jose, CA), rabbit anti-Tom40 antibody was purchased from Santa Cruz (Dallas, TX). Note that the expression of mitochondrial components in cyt $c^{-/-}$ cells were less than that in cyt $c^{+/+}$ cells.

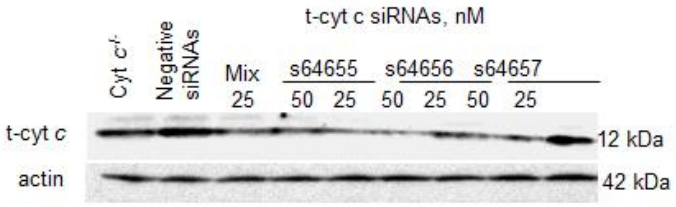

Figure S9c. Transient knock down of t-cyt *c* in s-cyt *c* deficient mouse embryonic (cyt $c^{-/-}$) cells using siRNA procedure. Cells were transfected with siRNAs (S64655, s64656, and s64657, respectively, final concentration, 25 and 50 nM, or a mixture of three siRNAs) against testicular cyt *c* (Ambion) using RNAiMax according to the manufacturer's instruction. Silencer Negative Control No. 1 siRNA (Ambion) was used as negative control. Cells were collected 72 hrs post-siRNA transfection, and resuspended in RIPA buffer for 30 min on ice. Supernatants were collected after 5 min centrifugation at 6,000 × g.

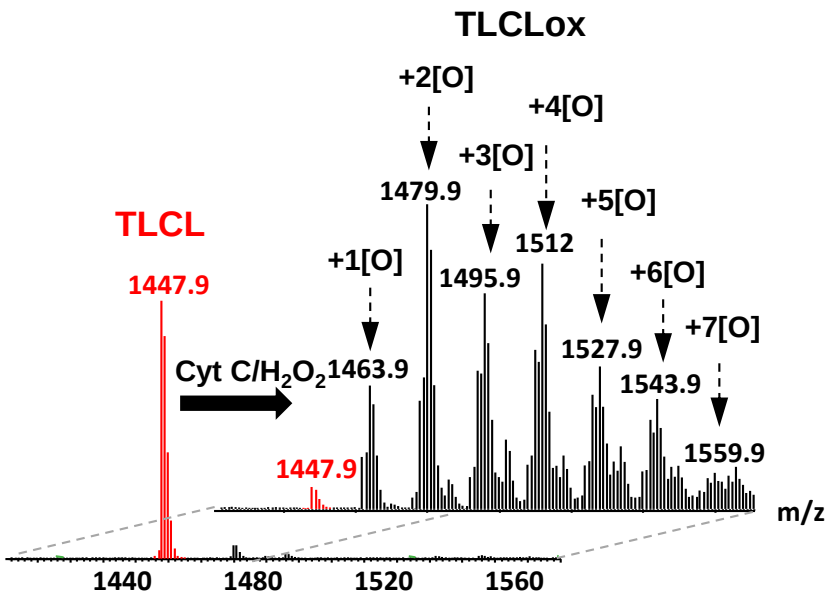

Figure S10. MS spectra of non-oxidized TLCL and $TLCL_{ox}$ formed in cyt *c* driven reaction in the presence of H_2O_2.

Table S6. Quantitative assessment of TLCL oxygenated species formed in cyt *c* driven reaction in the presence of H_2O_2. Data are mean ± S.D

m/z	Added Oxygen	% of total
1447.9	0	0.93±0.01
1461.9	1	2.17±0.09
1463.9	1	5.67±0.01
1477.9	2	4.75±0.21
1479.9	2	13.85±0.10
1493.9	3	6.23±0.17
1495.0	3	10.32±0.38
1509.9	4	7.22±0.26
1511.9	4	11.21±0.44
1525.9	5	5.52±0.03
1527.9	5	7.73±0.03
1541.9	6	5.80±0.72
1543.9	6	6.52±0.88
1557.9	7	3.08±0.55
1559.9	7	3.35±0.09
1573.9	8	2.13±0.46
1575.9	8	2.43±0.02
1589.0	9	0.55±0.03
1591.9	9	0.54±0.04

Table S7. Identification and quantitative assessment of major cardiolipin molecular species isolated from mouse brain.

m/z	CN:DB	Cardiolipin molecular species					pmol / nmol CL
		None	One PUFA	Two PUFAs	Three PUFA	Four PUFAs	
1428	70:4		$C_{16:0}C_{20:4}C_{16:0}C_{18:0}$ $C_{16:1}C_{20:3}C_{16:0}C_{18:0}$				41.2 ± 7.1
1448	72:8					$C_{18:2}C_{18:2}C_{18:2}C_{18:2}$	24.9 ± 3.7
1450	72:7		$C_{16:1}C_{16:0}C_{18:0}C_{22:6}$ $C_{16:1}C_{18:1}C_{20:4}C_{18:1}$ $C_{16:1}C_{20:4}C_{18:1}C_{18:1}$	$C_{16:1}C_{16:0}C_{20:3}C_{20:3}$ $C_{16:1}C_{18:1}C_{18:2}C_{20:3}$ $C_{16:0}C_{18:2}C_{20:4}C_{18:1}$ $C_{16:1}C_{20:4}C_{18:2}C_{18:0}$ $C_{16:1}C_{18:2}C_{20:3}C_{18:1}$ $C_{16:1}C_{18:2}C_{20:4}C_{18:0}$ $C_{16:0}C_{18:1}C_{18:2}C_{20:4}$ $C_{16:1}C_{18:0}C_{18:2}C_{20:4}$	$C_{16:0}C_{18:2}C_{18:2}C_{20:3}$		51.5 ± 3.5
1452	72:6			$C_{18:1}C_{18:2}C_{18:2}C_{18:1}$			52.0 ± 7.1
1454	72:5		$C_{16:1}C_{18:1}C_{20:3}C_{18:0}$ $C_{18:1}C_{18:1}C_{18:2}C_{18:1}$	$C_{18:1}C_{18:2}C_{18:2}C_{18:0}$			49.9 ± 8.4
1456	72:4	$C_{18:1}C_{18:1}C_{18:1}C_{18:1}$	$C_{18:1}C_{18:1}C_{18:2}C_{18:0}$				69.1 ± 7.1
1472	74:10			$C_{16:1}C_{20:4}C_{20:4}C_{18:1}$	$C_{16:1}C_{20:4}C_{20:3}C_{18:2}$ $C_{18:1}C_{18:2}C_{20:5}C_{18:2}$		27.9 ± 9.7
1474	74:9			$C_{16:0}C_{18:1}C_{18:2}C_{22:6}$			47.3 ± 6.4
1476	74:8		$C_{18:1}C_{18:1}C_{22:6}C_{16:0}$	$C_{18:0}C_{18:3}C_{20:4}C_{18:1}$ $C_{18:0}C_{18:2}C_{22:6}C_{16:0}$	$C_{18:1}C_{18:2}C_{20:3}C_{18:2}$ $C_{18:0}C_{18:3}C_{20:3}C_{18:2}$		61.1 ± 9.7
1478	74:7		$C_{16:0}C_{18:0}C_{22:6}C_{18:1}$ $C_{18:1}C_{18:1}C_{20:4}C_{18:1}$	$C_{18:1}C_{18:2}C_{20:4}C_{18:0}$ $C_{18:1}C_{18:2}C_{20:3}C_{18:1}$	$C_{18:0}C_{18:2}C_{20:3}C_{18:2}$		85.4 ± 7.6
1480	74:6		$C_{18:1}C_{18:1}C_{20:4}C_{18:0}$	$C_{18:0}C_{18:2}C_{20:4}C_{18:0}$			42.0 ± 4.2
1498	76:11			$C_{16:1}C_{20:3}C_{22:6}C_{18:1}$	$C_{18:2}C_{20:4}C_{20:4}C_{18:1}$		26.4 ± 2.0
1500	76:10			$C_{18:1}C_{20:4}C_{20:4}C_{18:1}$	$C_{18:2}C_{20:4}C_{20:4}C_{18:0}$		87.7 ± 7.9
1502	76:9			$C_{18:1}C_{20:4}C_{20:4}C_{18:0}$ $C_{18:1}C_{18:1}C_{20:4}C_{20:3}$	$C_{18:0}C_{18:2}C_{20:4}C_{20:3}$		58.9 ± 14.0
1504	76:8			$C_{18:1}C_{18:1}C_{20:3}C_{20:3}$			24.0 ± 3.4
1522	78:13				$C_{18:2}C_{22:4}C_{22:6}C_{18:1}$		21.2 ± 8.4
1524	78:12			$C_{18:1}C_{18:1}C_{20:4}C_{22:6}$ $C_{18:1}C_{20:4}C_{22:6}C_{18:1}$			51.3 ± 11.0
1526	78:11			$C_{18:1}C_{20:4}C_{22:5}C_{18:0}$	$C_{18:1}C_{18:2}C_{20:3}C_{22:5}$ $C_{18:0}C_{20:4}C_{22:5}C_{18:2}$		30.5 ± 3.3
1548	80:14			$C_{18:1}C_{22:6}C_{22:6}C_{18:1}$	$C_{18:0}C_{22:6}C_{22:6}C_{18:2}$		14.4 ± 7.4
1550	80:13			$C_{18:1}C_{22:6}C_{22:6}C_{18:0}$	$C_{18:0}C_{20:4}C_{22:6}C_{20:3}$ $C_{18:0}C_{20:3}C_{22:6}C_{20:4}$		6.7 ± 2.3

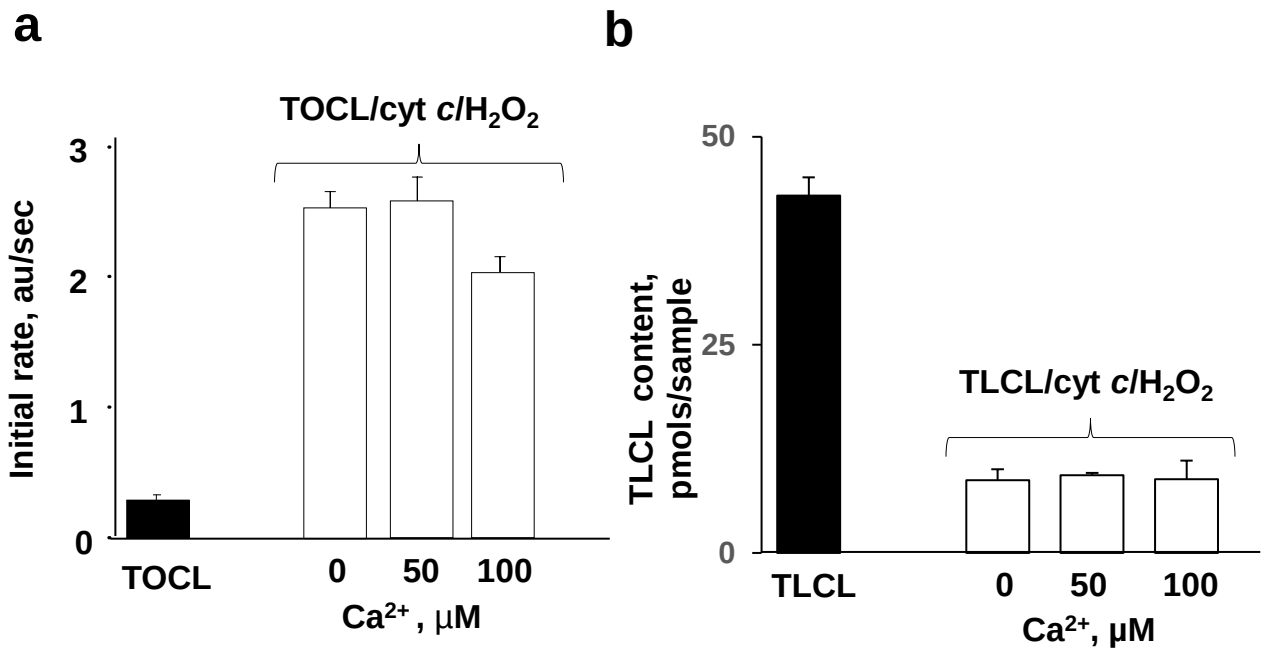

Figure S11. Effect of Ca^{2+} on peroxidase activity of cyt *c*/tetra-oleoyl-CL (TOCL) (a) and oxidation of TLCL by cyt *c* (b).

Peroxidase activity was measured in 25 mM HEPES buffer (pH 7.4) containing 100 μM DTPA. Concentration of TOCL was 50 μM, cyt *c* was 5 μM. Concentrations of Amplex Red and H_2O_2 were 100 μM. Fluorescence was measured using a Shimadzu RF5301-PC spectrofluorometer (λ_{ex}=575 nm and λ_{em}=585 nm).

For measurement of TLCL oxidation cyt *c* (5 μM) was incubated with TLCL containing liposomes (TLCL/cyt *c* ratio - 10:1) and H_2O_2 (100 μM) in 20 mM HEPES (pH 7.4) containing 100 μM DTPA for 10 min at 37°C. TLCL content was assessed by LC/MS and presented as pmols per sample.

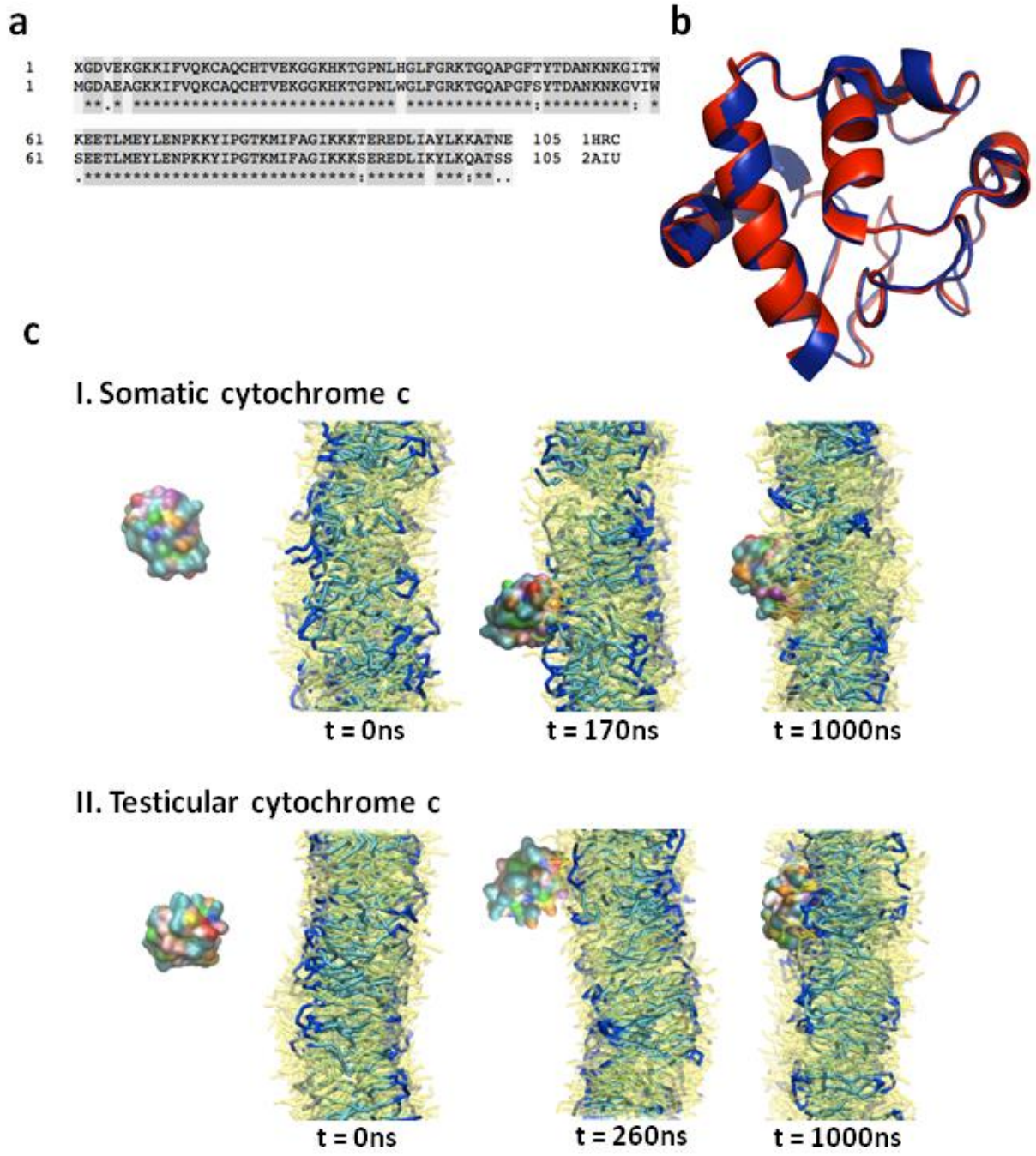

Figure S12. Comparison of somatic cyt *c* (s-cyt *c*) and testicular cyt *c* (t-cyt *c*). a. Sequence alignment of s-cyt c (pdb identifier 1HRC) and t-cyt c (pdb identifier 2AIU). These two isoforms share 88% identical residues. b. 3D structural alignment of s-cyt *c* (red) and t-cyt c (blue). The RMSD between these two structures is 0.36, demonstrating high structural similarity. c. Snapshots from coarse-grained molecular dynamics simulations of interaction of s-cyt *c* (Panel I) and t-cyt *c* (Panel II) with a TLCL-containing membrane. For clarity, water and ion molecules are not shown. Head groups of TLCL are shown as dark blue sticks, the acyl chains of CL as light blue sticks, DOPC as yellow, transparent sticks and the protein in each case is shown in colorful surface representation. The simulations demonstrate that both isoforms interact with the membrane in the early stages of the simulations, while they did not interact with membranes without CL (control simulations).

Table S8. Predicted binding energies of TLCL interacting with s-cyt c and t-cyt c. AutoDock Vina was used to predict top-ranking models for the interaction of TLCL with s-cyt c (pdb identifier 1HRC) and t-cyt c (pdb identifier 2AIU). Binding energies were comparable between the two structures. Color code: Green: residues appear in one or more models for both proteins; Red: residues that are unique for each protein and did not appear in any of the nine models for other protein.

Models	S-cyt c Residues by 5 Å of TLCL	Binding Energy (kCal/mol)	T-cyt c Residues by 5 Å of TLCL	Binding Energy (kCal/mol)
Model 1	Q12-K13-Q16-E69-N70-K72-I81-F82-A83-G84-I85-K86-K87-HEME	-2.6	E21-K22-G23-G24-H26-N31-W33-G34-F36-G37-R38-K39-Q42-A43-P44-G45-F46	-3.2
Model 2	K7-F10-V11-A15-H18-T19-V20-E21-K22-G23-G24-K25-K27-N31-H33-Y97-K100-A101-E104	-2.6	K7-K8-F10-V11-A15-H18-T19-V20-E21-K22-K27-W33-Y97-Q100-A101-S104	-3.2
Model 3	E21-K22-G23-G24-K25-H26-N31-H33-G34-R38-G41-Q42-A43-P44-G45-F46-K53-E104	-2.5	K7-K8-F10-V11-A15-T19-V20-E21-K22-G23-G24-K25-K27-W33-Y97-Q100-A101-S104	-3.2
Model 4	K7-F10-V11-A15-Q16-H18-T19-V20-E21-K22-K25-K27-Y97-K100-A101-E104	-2.5	E4-A5-K7-K8-I9-F10-V11-Q12-K13-A15-Q16-H18-T19-V20-E21-K22-G24-K25-K27-E90-Y97-Q100-A101	-3.2
Model 5	E21-K22-G23-G24-H26-N31-H33-G34-L35-F36-G37-R38-K39-Q42-P44-K53-N54-G56-T102-N103-E104	-2.5	E21-K22-G23-G24-H26-N31-W33-G34-F36-G37-R38-Q42-A43-P44-G45-F46-T102-S103-S104	-3.1
Model 6	E4-K7-K8-F10-V11-Q12-K13-A15-Q16-H18-T19-V20-E21-K25-K27-Y97	-2.5	K7-F10-V11-A15-H18-T19-V20-E21-K22-K25-K27-W33-Y97-Q100-A101-S104	-3.0
Model 7	Q12-K13-Q16-C17-H26-K27-T28-G29-G45-F46-T47-Y48-T49-D50-K53-K79-I81-F82-A83-HEME	-2.4	E21-K22-G23-G24-H26-N31-W33-G34-F36-G37-R38-Q42-A43-P44-G45-F46-T102-S103	-3.0
Model 8	K7-F10-V11-A15-H18-T19-V20-E21-K22-K25-K27-H33-Y97-K100-A101-E104	-2.4	E4-K7-K8-F10-V11-A15-H18-T19-V20-E21-K22-K25-K27-W33-Y97-Q100-A101-S104	-3.0
Model 9	E21-K22-G23-G24-K25-H26-N31-H33-G34-F36-G37-R38-K39-G41-Q42-A43-P44-G45-F46-T47-Y48-K53	-2.4	K7-F10-V11-A15-T19-V20-E21-K22-K27-W33-Y97-Q100-A101-S104	-2.9

Supplementary Methods

Treatment of mice. Mice were treated with mixture of inhibitors (COX-1 and COX-2 inhibitor - piroxicam (4-hydroxy-2-methyl-N-2-pyridinyl-2H-1,2-benzothiazine-3-carboxam, ide-1,1-dioxide, 30 mg/kg of body weight), dual COX/LOX inhibitor- licophelone (6-(4-chlorophenyl)-2,3-dihydro-2,2-dimethyl-7-phenyl-1H-pyrrolizine-5-acetic acid, 10 mg/kg of body weight), and inhibitor of cytochrome P450 - MS-PPOH (N-(methylsulfonyl)-2-(2-propynyloxy)-benzenehexanamide, 25 mg/kg of body weight) by oral gavage 2 hrs prior irradiation. Control mice and mice pretreated with drugs were exposed to WBI (10Gy) and sacrificed 24 hrs thereafter. Data are presented as % of particular FA_{ox} accumulated in irradiated non-treated mice. To inhibit Ca^{2+}-independent $iPLA_2$, mice were treated with R-BEL, (6E-(bromoethylene)tetrahydro-3R-(1-naphthalenyl)-2H-pyran-2-one, (R)-bromoenol lactone) at dose of 6 mg/kg body weight by I.P. 6 hrs prior to WBI. All procedures were approved by the IACUC of University of Pittsburgh and performed according to the established protocols.

Mitochondria were isolated from either C57BL/6J mouse heart or liver using differential centrifugation. Heart mitochondria (1 mg protein/mL) were exposed to *t*-BuOOH (150 μM) for 1 h at 37ºC. Liver mitochondria were used in experiments on hydrolysis of exogenous $TLCL_{ox}$ by mitochondrial $iPLA_2$. Briefly, $TLCL_{ox}$ (30 nmol/mg protein) was added to mitochondria homogenates (0.5 mg protein/mL), which were then resuspended in 50 mM HEPES buffer, pH 7.8, containing 10 mM KCl, 1 mM EGTA, 1 mM DTT, 100 μM DTPA and 10% glycerol and incubated for 1 h at 37ºC. To inhibit Ca^{2+}-independent PLA_2 selective inhibitor, (R)-bromoethol lactone ((R)-BEL) (30 nmol/mg protein) was added 5 min prior to the addition of $TLCL_{ox}$.

Cell culture: Mouse embryonic cyt $c^{-/-}$ cells (ATCC) and cyt $c^{+/+}$ cells (courtesy of Dr. Xiaodong Wang, Department of Biochemistry, University of Texas, Southwestern Medical Center, Dallas, TX) were cultured in DMEM supplemented with 15% FBS, 25 mM HEPES, 50 mg/L uridine, 110 mg/L pyruvate, 2 mM glutamine, 1×nonessential amino acids, 0.05 mM 2′-mercaptoethanol, 0.5×10^6 U/L mouse leukemia inhibitory factor and 100 U/ml penicillin and streptomycin. Cyt $c^{-/-}$ and cyt $c^{+/+}$ mouse embryonic cells were exposed to either ActD (100 ng/mL) for 16 h at 37ºC or *t*-BOOH (200 μM) for 16 h at 37ºC. PS externalization was determined with the Annexin V-FITC Apoptosis Detection Kit (BioVision, Mountain View, CA).

SiRNA procedure. Transient knocking down of testicular cyt *c* in somatic cyt *c* deficient mouse embryonic (cyt $c^{-/-}$) cells was achieved by siRNA procedure. Cells were transfected with siRNAs

(Ambion, S64655, s64656, and s64657, respectively, final concentration, 25 and 50 nM, or a mixture of three siRNAs, 25 nM final) against testicular cyt *c* using RNAiMax (Invitrogen) according to the manufacturer's instruction. Silencer Negative Control No. 1 siRNA (Ambion) was used as negative control. Cells were collected 72 hrs post-siRNA transfection for further experiments.

Western blotting. Whole cell lysates were obtained by re-suspending cells in RIPA buffer for 30 min on ice. Supernatants were collected after 5-min centrifugation at 6,000 × g. The resulting supernatants were subjected to 15% SDS-PAGE and then transferred to nitrocellulose membrane. The membrane was blocked with fat-free milk and probed with antibodies against testicular-cyt *c* (Rabbit anti-t-cyt *c* antibody was courtesy of Dr. Millan, Sanford-Burnham Medical Research Institute, LaJolla, CA), MnSOD (BD, San Jose, CA), Tim-23 (BD), Tim40 (Santa Cruz, Dallas, Texas) and β-actin (loading control, Sigma, St. Louis, MO) followed by horseradish peroxidase-coupled detection. Recombinant t-cyt *c* was from Creative Biomart (Shirley, NY). Quantification of band intensity was performed using ImageJ pixel analysis (NIH Image software, Ver. 1.47). The cellular content of t-cyt *c* was calculated based on the calibration, and normalized to the amount of protein loaded.

Neuron culture. Timed pregnant Sprague Dawley rats were euthanized by CO_2 asphyxiation/decapitation and embryos rapidly isolated. Embryonic brains were removed, placed in 10cm dishes containing ice cold hanks balanced salt solution (HBSS; supplemented with HEPES, Sodium Bicarbonate, and Penicillin(Pen)/Streptomycin(Strep)), and cortical tissue separated under a dissecting microscope. Cortical tissue was minced with scissors in a 1.5mL sterile tube for ~2mins. Dissociated brain was transferred into a 15mL conical tube and spun at 200g/4°C/5min. The pellet was resuspended in 2mL of trypsinization solution (1mg/mL trypsin + 4mg/mL DNaseI dissolved in HBSS), transferred to a 50mL conical tube, and gently rocked in a 37°C water bath for 8mins. 10mL of quenching solution (Neurobasal/B27/10% heat-inactivated FBS) was added to stop trypsin reaction, and cells transferred into a new 15mL conical tube. Cells were spun at 200g/4°C/5min. The cell pellet was resuspended in 2mL of trituration solution (10mg DNaseI/mL dissolved in Neurobasal/B27). Cells were further dissociated by 10 strokes through a fire-polished glass Pasteur pipette. Cells were spun once more at 200g/4°C/5min, and resuspended in 10mL neuronal plating media (Neurobasal/B27 + 25μM glutamic acid + L-Glutamine + Pen/Strep). Neurons were counted using a hemacytometer, and seeded onto 10cm culture dishes (treated overnight with poly-D-lysine) at ~5-10X10^6. At day in vitro (DIV) 3, half of the media was replaced with fresh Neurobasal/B27 (without glutamic acid). Neurons were injured at DIV6.

Astrocyte culture. Brain tissue for astrocytes was harvested from the same embryo isolations used for neuron cultures (to control for genetic variations between animals). Tissue was collected into a 15mL tube. 4mg/mL DNase I was dissolved into 0.25% trypsin-EDTA solution (Life Technologies). Brain tissue was dissociated in a 0.25%Trypsin/EDTA solution (Life Technologies) and incubated 10 min at 37°C. Brain tissue was triturated/dissociated 20-30X in a 50mL tube using a 10mL pipette. Trypsin was quenched using regular astrocyte growth media (DMEM/F12/10%FBS + HEPES + Pen/Strep), cells spun at 200g/4 °C/5min, and pellet resuspended in regular growth media. Mixed cell population (i.e. total brain) was seeded onto T-75 flasks. To extract pure astrocytes, cells were grown to confluence, and propagated several times by seeding at low density (only astrocytes exponentially proliferate). Fresh growth/maintenance media was replaced every 3-4 days. After 2-3 propagations pure astrocytes were split and seeded onto poly-D-lysine coated 10cm dishes. Injury experiments were started when astrocytes reached ~70-80% confluence.

Hydrogen peroxide treatment. Neurons and astrocytes were exposed to H_2O_2 identical conditions. Cells were washed twice with a modified Balanced Salt Solution (BSS) containing 5mM glucose to remove antioxidants present in growth media. 10µL of 30% concentrated H_2O_2 was dissolved in 10mL sterile double-distilled H_2O (ddH_2O) (Stock 1). Stock 1 was directly added to a BSS (i.e. cell treatment media) (final H_2O_2 concentration 40µM) and samples were incubated for 3hrs at 37 ^oC. Controls received an equal volume of ddH_2O in BSS but without any H_2O_2. All H_2O_2 treatments were applied within 3-4mins after preparation in sterile water/BSS. After 3h, cells were harvested in 400µL PBS, immediately spun at 200g/4 °C/5min, frozen on dry ice, and transferred to a -80°C ultra-low until lipid analysis.

Isolation of CL from mouse brain and its oxidation by cyt c. Total lipids were extracted from mouse brain using Folch procedure [16]. CL was separated by HPLC as previously described [17]. The purity of isolated CL was confirmed by LC-MS as described below. CL (250 µM) was re-suspended in 20 mM HEPES buffer pH 7.4, containing 100 µM DTPA and sonicated on ice-water for 20 min using high performance ultrasonic system FS3 (Fisher Scientific, PA). After that cyt *c* (10 µM) and H_2O_2 (100 µM) were added and samples were incubated up to 3h at 37 ^oC. Cyt *c* and H_2O_2 were added every 10 min. At the end of incubation CL was extracted and analyzed by LC-MS.

Oxidation of TLCL by cyt c and H_2O_2. Tetra-linoleoyl-cardiolipin (TLCL) (250 µM) (Avanti Polar Lipids Inc., Alabaster, AL) was re-suspended in 20 mM HEPES buffer pH 7.4, containing 100 µM DTPA. Cyt *c* (10 µM) and H_2O_2 (100 µM) were added to TLCL and samples were incubated up to 1h at 37 ^oC. Cyt c

and H_2O_2 were added every 10 min. At the end of incubation a mixture of TLCL and $TLCL_{ox}$ was separated by LC/MS as described previously [17].

Hydrolysis of CL by phospholipases A_1 and A_2. To identify FA oxidation species, CLs were treated with phospholipase A_1 (PLA_1) from *Thermomyces lanuginosus* (10 µl/µmol CL) (Sigma-Aldrich, St. Louis, MO) and phospholipase A_2 (PLA_2) from porcine pancreas (10U/µmol of CL) (Sigma-Aldrich, St. Louis, MO) in 0.5 M borate buffer, pH 9.0 containing 20 mM cholic acid, 2 mM $CaCl_2$ and 100 µM DTPA for 60 min and liberated FA and FA_{ox} were extracted by Folch procedure[16] and analyzed by LC/MS. Under these conditions, almost 99% of CLs were hydrolyzed.

Hydrolysis of TLCL and oxygenated TLCL by PAF-AH. $TLCL_{ox}$ (2.6 µmol/mL) was incubated in the presence of PAF-AH (3 mUnits/mL) (Cayman Chemical, Ann Arbor, MI) in 50 mM HEPES buffer, pH 7.8, containing 100 µM DTPA for 1 h at 37°C. PAF-AH was added three times (every 15 min of incubation). At the end of incubation lipids were extracted and analyzed by LC/MS.

Standards used: 9-hydroperoxy-10E,12Z-octadecadienoic acid (9-HpODE), 13-hydroperoxy-9Z,11E-octadecadienoic acid (13-HpODE), 9-hydroxy-10E,12Z-octadecadienoic acid (9-HODE), 13-hydroxy-9Z, 11E-octadecadienoic acid (13-HODE), 9-oxo-10E,12Z-octadecadienoic acid (9-KODE), 13-oxo-9Z,11E-octadecadienoic acid (13-KODE), 9(10)-epoxy-12Z-octadecenoic acid (9,10-EpOME) 12(13)epoxy-9Z-octadecenoic acid (12,13-HpOME) (±)14,15-dihydroxy-5Z, 8Z, 11Z-eicosatrienoic acid (14,15-DiHETrE), (±)11,12-dihydroxy-5Z, 8Z, 14Z-eicosatrienoic acid (11,12-DiHETrE), (±)8,9-dihydroxy-5Z, 8Z, 14Z-eicosatrienoic acid (8,9-DiHETrE), (±)5,6-dihydroxy-8Z, 11Z, 14Z-eicosatrienoic acid (5,6-DiHETrE), 20-hydroxy-5Z, 8Z, 11Z, 14Z-eicosatetraenoic acid (20-HETE), 20-hydroxy-5Z, 8Z, 11Z, 14Z-eicosatetraenoic-16,16,17,17,18,18-d6 acid (20-HETE-d6), 19S-hydroxy-5Z, 8Z, 11Z, 14Z-eicosatetraenoic acid (19-HETE), 18S-hydroxy-5Z, 8Z, 11Z, 14Z-eicosatetraenoic acid (18-HETE), 17S-hydroxy-5Z, 8Z, 11Z, 14Z-eicosatetraenoic acid (17-HETE), 16S-hydroxy-5Z, 8Z, 11Z, 14Z-eicosatetraenoic acid (16-HETE), 15S-hydroxy-5Z, 8Z, 11Z, 13E-eicosatetraenoic acid (15-HETE), 12S-hydroxy-5Z, 8Z, 10E, 14Z-eicosatetraenoic acid (12-HETE), (±)11-hydroxy-5Z,8Z,12E,14Z-eicosatetraenoic acid (11-HETE), (±)-9-hydroxy-5Z,7E,11Z,14Z-eicosatetraenoic acid (9-HETE), (±)8-hydroxy-5Z,9E,11Z,14Z-eicosatetraenoic acid (8-HETE), (±)5-hydroxy-6E,8Z,11Z,14Z-eicosatetraenoic acid (5-HETE), (±)14(15)-epoxy-5Z, 8Z, 11Z-eicosatrienoic acid (14,15-EET), (±)11(12)-epoxy-5Z, 8Z, 14Z-eicosatrienoic acid (11,12-EET), and (±)8(9)-epoxy-5Z, 11Z, 14Z-eicosatrienoic acid (8,9-EET), (±)9(10)-dihydroxy-12Z-octadecenoic acid (9,10-DiHOME), (±)9(10)-epoxy-12Z-octadecenoic acid (9,10-EpOME) purchased from Cayman chemicals (Ann Arbor, MI).

Assessment of peroxidase activity of cyt *c*. Assessment of peroxidase activity with Amplex Red reagent was performed by measuring the fluorescence of resorufin, an oxidation product of Amplex Red in 25 mM HEPES buffer (pH7.4) containing 100 µM DTPA. Small unilamellar liposomes were prepared from di-oleoyl-phosphatidylcholine (DOPC) (Avanti Polar Lipids Inc., Alabaster, AL) and tetra-oleoyl-cardiolipin (TOCL) (Avanti Polar Lipids Inc., Alabaster, AL) (1:1 ratio). Individual phospholipids, stored in chloroform, were mixed and dried under nitrogen. Then lipids were mixed in vortex in HEPES buffer (20 mM, pH 7.4) and sonicated on ice. Liposomes were used immediately after preparation. Cyt *c* (5 *µ*M) was incubated with liposomes (TOCL/cyt c ratio 10:1) for 10 min in the presence and in the absence of $CaCl_2$ (50 and 100 µM). Peroxidase reaction was started by addition of Amplex Red (100 *µ*M) and H_2O_2 (100 *µ*M). Fluorescence was measured using a Shimadzu RF5301-PC spectrofluorometer (λ_{ex}=575 nm and λ_{em}=585 nm). To estimate the effect of calcium on CL oxidation, cyt *c* (5 µM) was incubated with TLCL containing liposomes (TLCL/cyt *c* ratio - 10:1) and H_2O_2 (100 µM) in 20 mM HEPES (pH 7.4) containing 100 µM DTPA for 10 min at 37^{o}C. CL was extracted by Folch procedure and analyzed by LC/MS.

Sequence and 3D structure alignments. Sequences were extracted from the uniprot database[18]. The two isoforms of cyt c show 88% identical resides. Structure alignment was carried out using PDBeFold[19].

Molecular docking. TLCL was docked to the crystal structure of s-cyt c (PDBid:1HRC[20]) and t-cyt c (PDBid:2AIU[21]) using AutoDock Vina[22]. Lipid and protein structures were converted from pdb into pdbqt format using MGL Tools[23]. In both cases, the 9 top-ranked binding poses with the highest binding affinities were reported (Supplemental Table S6).

Coarse-grained molecular dynamics (CGMD) simulations. CGMD simulations of lipid bilayer systems were carried out using the MARTINI force field[24], essentially as described previously[25]. The lipid bilayer was composed of DOPC and ~20% TLCL. Three CGMD simulations, employing different initial velocities with identical initial configurations, were performed to study the interactions of s-cyt c and t-cyt c with TLCL-containing bilayers in addition to three control simulations using the bilayer without TLCL. All simulations were performed using the GROMACS v. 4.5.4 MD package[26] and visualized using the VMD v. 1.9 software[27]. Initially, the system was minimized for 20 ps, before 0.2 ns NPT ensemble equilibration followed by a 0.2ns NVT ensemble equilibration. Each CGMD run was carried out for 1 µs. A 20 fs time step was used to integrate the equations of motion. Non-bonded interactions have a cutoff distance of 1.2nm. Temperature and pressure were controlled using the velocity rescale (V-rescale)[28]

and Berendsen[29] algorithms, respectively. Simulations were run at 300K and at 1atm during NPT runs. For all CGMD simulations, elastic networks were used to preserve the protein structures[30, 31].

Statistics. The data are presented as mean ± S.D. values from at least three experiments. Statistical analyses were performed by either unpaired Student's *t*-test or one-way ANOVA. The statistical significance of differences was set at $p< 0.05$.

Supplementary References

1. Patwardhan, A.M., Scotland, P.E., Akopian, A.N. & Hargreaves, K.M. Activation of TRPV1 in the spinal cord by oxidized linoleic acid metabolites contributes to inflammatory hyperalgesia. *Proc Natl Acad Sci U S A* **106**, 18820-18824 (2009).
2. Altmann, R. *et al.* 13-Oxo-ODE is an endogenous ligand for PPARgamma in human colonic epithelial cells. *Biochemical pharmacology* **74**, 612-622 (2007).
3. Vangaveti, V., Baune, B.T. & Kennedy, R.L. Hydroxyoctadecadienoic acids: novel regulators of macrophage differentiation and atherogenesis. *Therapeutic advances in endocrinology and metabolism* **1**, 51-60 (2010).
4. Alsalem, M. *et al.* The contribution of the endogenous TRPV1 ligands 9-HODE and 13-HODE to nociceptive processing and their role in peripheral inflammatory pain mechanisms. *British journal of pharmacology* **168**, 1961-1974 (2013).
5. Obinata, H., Hattori, T., Nakane, S., Tatei, K. & Izumi, T. Identification of 9-hydroxyoctadecadienoic acid and other oxidized free fatty acids as ligands of the G protein-coupled receptor G2A. *The Journal of biological chemistry* **280**, 40676-40683 (2005).
6. Goodfriend, T.L., Ball, D.L., Egan, B.M., Campbell, W.B. & Nithipatikom, K. Epoxy-keto derivative of linoleic acid stimulates aldosterone secretion. *Hypertension* **43**, 358-363 (2004).
7. Huang, J.T. *et al.* Interleukin-4-dependent production of PPAR-gamma ligands in macrophages by 12/15-lipoxygenase. *Nature* **400**, 378-382 (1999).
8. Delerive, P. *et al.* Oxidized phospholipids activate PPARalpha in a phospholipase A2-dependent manner. *FEBS letters* **471**, 34-38 (2000).
9. Morgantini, C. *et al.* Apolipoprotein A-I mimetic peptides prevent atherosclerosis development and reduce plaque inflammation in a murine model of diabetes. *Diabetes* **59**, 3223-3228 (2010).
10. Pidgeon, G.P. *et al.* Lipoxygenase metabolism: roles in tumor progression and survival. *Cancer Metastasis Rev* **26**, 503-524 (2007).
11. Rankin, J. Cerebral vascular accidents in patients over the age of 60. II. Prognosis. *Scottish medical journal* **2**, 200-215 (1957).
12. Setty, B.N., Werner, M.H., Hannun, Y.A. & Stuart, M.J. 15-Hydroxyeicosatetraenoic acid-mediated potentiation of thrombin-induced platelet functions occurs via enhanced production of phosphoinositide-derived second messengers--sn-1,2-diacylglycerol and inositol-1,4,5-trisphosphate. *Blood* **80**, 2765-2773 (1992).
13. Pearson, T., Warren, A.Y., Barrett, D.A. & Khan, R.N. Detection of EETs and HETE-generating cytochrome P-450 enzymes and the effects of their metabolites

on myometrial and vascular function. *American journal of physiology. Endocrinology and metabolism* **297**, E647-656 (2009).
14. Spector, A.A. & Norris, A.W. Action of epoxyeicosatrienoic acids on cellular function. *American journal of physiology. Cell physiology* **292**, C996-1012 (2007).
15. Roman, R.J. P-450 metabolites of arachidonic acid in the control of cardiovascular function. *Physiological reviews* **82**, 131-185 (2002).
16. Folch, J., Lees, M. & Sloane Stanley, G.H. A simple method for the isolation and purification of total lipides from animal tissues. *The Journal of biological chemistry* **226**, 497-509 (1957).
17. Samhan-Arias, A.K. *et al.* Oxidized phospholipids as biomarkers of tissue and cell damage with a focus on cardiolipin. *Biochim Biophys Acta* **1818**, 2413-2423 (2012).
18. Apweiler, R. *et al.* Update on activities at the Universal Protein Resource (UniProt) in 2013. *Nucleic acids research* **41**, D43-D47 (2013).
19. Krissinel, E. & Henrick, K. Secondary-structure matching (SSM), a new tool for fast protein structure alignment in three dimensions. *Acta crystallographica. Section D, Biological crystallography* **60**, 2256-2268 (2004).
20. Bushnell, G.W., Louie, G.V. & Brayer, G.D. High-resolution three-dimensional structure of horse heart cytochrome c. *Journal of molecular biology* **214**, 585-595 (1990).
21. Liu, Z. *et al.* Remarkably high activities of testicular cytochrome c in destroying reactive oxygen species and in triggering apoptosis. *Proc Natl Acad Sci U S A* **103**, 8965-8970 (2006).
22. Trott, O. & Olson, A.J. AutoDock Vina: improving the speed and accuracy of docking with a new scoring function, efficient optimization, and multithreading. *Journal of computational chemistry* **31**, 455-461 (2010).
23. Sanner, M.F. Python: a programming language for software integration and development. *Journal of molecular graphics & modelling* **17**, 57-61 (1999).
24. Marrink, S.J., Risselada, H.J., Yefimov, S., Tieleman, D.P. & de Vries, A.H. The MARTINI force field: coarse grained model for biomolecular simulations. *The journal of physical chemistry. B* **111**, 7812-7824 (2007).
25. Chu, C.T. *et al.* Cardiolipin externalization to the outer mitochondrial membrane acts as an elimination signal for mitophagy in neuronal cells. *Nature cell biology* **15**, 1197-1205 (2013).
26. Van Der Spoel, D. *et al.* GROMACS: fast, flexible, and free. *Journal of computational chemistry* **26**, 1701-1718 (2005).
27. Humphrey, W., Dalke, A. & Schulten, K. VMD: visual molecular dynamics. *Journal of molecular graphics* **14**, 33-38, 27-38 (1996).
28. Bussi, G., Donadio, D. & Parrinello, M. Canonical sampling through velocity rescaling. *Journal of Chemical Physics* **126** (2007).
29. Berendsen, H.J.C., Postma, J.P.M., Vangunsteren, W.F., Dinola, A. & Haak, J.R. Molecular-Dynamics with Coupling to an External Bath. *Journal of Chemical Physics* **81**, 3684-3690 (1984).
30. Arnarez, C., Mazat, J.P., Elezgaray, J., Marrink, S.J. & Periole, X. Evidence for cardiolipin binding sites on the membrane-exposed surface of the cytochrome bc1. *Journal of the American Chemical Society* **135**, 3112-3120 (2013).
31. Periole, X., Cavalli, M., Marrink, S.J. & Ceruso, M.A. Combining an Elastic Network With a Coarse-Grained Molecular Force Field: Structure, Dynamics, and Intermolecular Recognition. *J Chem Theory Comput* **5**, 2531-2543 (2009).